processes

MDPI

Article

Effect of Obstacle Gradient on the Deflagration Characteristics of Hydrogen/Air Premixed Flame in a Closed Chamber

Yufei Wang and Shengjun Zhong *

School of Metallurgy, Northeastern University, Shenyang 110819, China; 2101636@stu.neu.edu.cn
* Correspondence: zhongsj@smm.neu.edu.cn; Tel.: +86-15524007116

Abstract: In this paper, computational fluid dynamics (CFD) numerical simulation is employed to analyze and discuss the effect of obstacle gradient on the flame propagation characteristics of premixed hydrogen/air in a closed chamber. With a constant overall volume of obstacles, the obstacle blocking rate gradient is set at +0.125, 0, and −0.125, respectively. The study focuses on the evolution of the flame structure, propagation speed, the dynamic process of overpressure, and the coupled flame–flow field. The results demonstrate that the flame front consistently maintains a jet flame as the obstacle gradient increases, with the wrinkles on the flame front becoming increasingly pronounced. When the blocking rate gradients are +0.125, 0, and −0.125, the corresponding maximum flame propagation speeds are measured at 412 m/s, 344 m/s, and 372 m/s, respectively, indicating that the obstacle gradient indeed increases the flame propagation speed. Moreover, the distribution of pressure is closely related to changes in the flame structure, with the overpressure decreasing in the obstacle channel as the obstacle gradient increases. Furthermore, the velocity vector and vortex distribution in the flow field are revealed and compared. It is found that the obstacle tail vortex is the main factor inducing flame evolution and flow field changes in a closed chamber. The effect of the blocking rate gradient on flow velocity is also quantified, with instances of deceleration occurring when the blocking rate gradient is −0.125.

Keywords: premixed flame; obstacle gradient; numerical simulation; flow field

Citation: Wang, Y.; Zhong, S. Effect of Obstacle Gradient on the Deflagration Characteristics of Hydrogen/Air Premixed Flame in a Closed Chamber. *Processes* **2024**, *12*, 962. https://doi.org/10.3390/pr12050962

Academic Editor: Albert Ratner

Received: 9 April 2024
Revised: 27 April 2024
Accepted: 7 May 2024
Published: 9 May 2024

1. Introduction

Hydrogen energy, as a clean, green, low-carbon, and sustainable new energy carrier, has been widely used worldwide [1–5]. However, due to its low density, high diffusivity, wide range of flammability limits, low ignition energy, and high flame propagation rate [6,7], hydrogen presents potential leakage during its preparation, storage, transport, and application, which can form substantial explosive mixtures even in open areas [8]. Once an ignition source is encountered, a fast-turbulent deflagration will occur at ultra-high pressure, with the acceleration effect caused by obstacle-induced turbulence being particularly significant, facilitating the flame transition from deflagration to detonation (DDT) [9,10]. The sharp increase in temperature and pressure during the explosion and the generation of strong shock waves can cause severe casualties and damage [11–13], triggering a series of hydrogen safety accidents [8,14].

Therefore, studying the acceleration mechanism of obstacle-induced flames is essential to prevent flame acceleration and DDT formation [15,16]. The study of combustion and explosion of channel obstacles has become an important topic, for which scholars have researched premixed gas explosions related to obstacle-related factors. Currently, the problems associated with the explosion behavior of fuel/air in an obstructed chamber can generally be classified into two categories: the mechanism of flame acceleration induced by obstacles, and the effects of the number, blocking rate (BR), and shape of obstacles.

Many studies have explained the mechanism of how obstacles affect flame dynamics. Boeck et al. [17] pointed out that the vortex flame interaction is the fundamental cause

of flame wrinkling. Yang et al. [18] conducted an experiment using a closed rectangular pipeline and identified that the presence of obstacles can change the shape of the flame tip and damage the flame surface. After passing through the obstacles, the flame will still reverse to form a tulip flame which will have a new development mode due to the vortex motion caused by the obstacle. Xiao et al. [19] investigated and compared the effects of various obstacles on DDT in pipelines, and found that flames would wrinkle when encountering obstacles, leading to a transition from laminar to turbulent combustion. Oh et al. [20] discovered that the momentum of vortex triggered by the obstacles will first slow down after passing through an obstacle. And the turbulent flame combustion intensifies and the flame speed increases after the vortex is broken. Among the above studies, it is generally believed that the evolution of the flame structure and explosion characteristic parameters caused by obstacles are jointly influenced by the turbulent positive feedback mechanism and vortex flame interaction.

Furthermore, the effects of the number of obstacles, blockage rate (BR), spacing, and shape on the flame acceleration were studied. Qin et al. [21] analyzed that explosive flames under obstacles with different numbers conform to typical self-similarity. And the more obstacles there are, the stronger the fluid instability formed. Elshimy M. [22] and Qin [23] used numerical simulations to discuss the effect of different obstacle blocking rates on explosion flames. They concluded that an increase in obstacle blocking rates would enhance the explosion overpressure, and the structure of flames after passing through obstacles was generally the same under different blocking rate conditions. However, Mei et al. [24] investigated the explosion characteristics of premixed hydrogen under obstacles of different shapes and blocking rates. The results indicated that the flame front will not recover to a regular front after passing through many gap grid obstacles. Sheng et al. [15] revealed the effects of three different shaped obstacles, namely, triangles, squares, and circles, on premixed flames. They pointed out that the peak overpressure caused by triangular obstacles was 7% and 30% higher than that of square and circular obstacles, respectively. Jiang et al. [25] indicated through experiments and simulations to analyze and compare the effects of obstacles at different positions on hydrogen explosion flames. It was found that with the increase in obstacle distance, the turbulent combustion, flame backflow, and overpressure were significantly enhanced. The flame vortex interaction caused strong turbulent combustion and rapid overpressure growth.

Yet, due to the complexity of scenarios in actual pipeline transportation and industrial applications, the arrangement of obstacles in pipelines has also attracted the interest of many scholars. Wang et al. [26] confirmed that with the increase in obstacle channels, the degree of flame folding increases. The flame propagation process is mainly affected by fluid dynamic instability and eddy currents. Xiu et al. [27] explored the evolution process of explosion flame propagation in hydrogen/air premixed systems by increasing the number of obstacles in the obstacle channel. They explored that the flame propagation speed and flame front area is increased with the increase in obstacles, and the flame front area showed a logarithmic relationship with the number of obstacles. Zheng et al. [28] further incorporated experiments on the explosion of methane at different concentrations in obstacle gradient pipelines, and the results showed that blocking rate gradients significantly affect the evolution structure of flame, propagation speed, and overpressure.

Under the condition of obstacles, a considerable number of experimental and numerical simulation studies have been carried out on the gas explosion behavior. However, the current research almost focuses on the shape, spacing, arrangement, and location of obstacles. In addition, the influence of single obstacle and multiple obstacles on the behavior of gas explosion is under the condition of a fixed blocking rate. The evolution of the gas explosion flame and obstacle-induced flame acceleration behavior have only been studied by a few scholars [28,29] (the fuel is mainly methane), under the continuous obstacles with variable blocking rate, which happens to be a common situation in actual hydrogen applications, such as complex equipment in workshops, pipeline transportation, and vehicles in tunnels. Also, the effect of the varying blocking rate (barrier volume is

constant) on the explosion behavior of hydrogen/air premixed flame in confined space has never been investigated.

Therefore, in this paper, we develop multiple obstacle gradient conditions by changing the arrangement of obstacles. Furthermore, the evolution process of hydrogen/air explosion flame behavior in a closed chamber is revealed through numerical simulation. The research results can provide theoretical guidance for the safe use of hydrogen in confined space and field design. Meanwhile, the research can fill the knowledge gap in the impact of obstacle on hydrogen/air explosion.

2. Numerical Methods

2.1. Governing Equation

The explosion of premixed gas is essentially a rapid chemical reaction process, so the following basic assumptions are made in this study [21,30]:

- The premixed gas is uniformly distributed before ignition.
- The wall is a non-slip and adiabatic boundary.
- The effects of gravity, thermal radiation, and heat loss are neglected owing to the reaction time being extremely short.
- The explosion gas is treated as a compressible ideal gas.

The explosion process can be described using the unsteady N-S equation as follows [23,26,31,32]:

The mass conservation equation is:

$$\frac{\partial \rho}{\partial t} + \nabla \cdot (\rho \vec{v}) = 0 \tag{1}$$

The momentum conservation equation is:

$$\frac{\partial}{\partial t}(\rho \vec{v}) + \nabla \cdot (\rho \vec{v}\vec{v}) = -\nabla p + \nabla \cdot (\overline{\overline{\tau}}) \tag{2}$$

$$\overline{\overline{\tau}} = \mu \left[\left(\nabla \vec{v} + \nabla \vec{v}^T \right) - \frac{2}{3} \nabla \cdot \vec{v} I \right] \tag{3}$$

The energy conservation equation is:

$$\frac{\partial}{\partial t}\left(\rho\left(e + \frac{v^2}{2}\right)\right) + \nabla \cdot \left(\rho v \left(h + \frac{v^2}{2}\right)\right) = \nabla \cdot \left(k_{eff} \nabla T - \sum_j h_j \vec{J}_j + \overline{\overline{\tau}}_{eff} \cdot \vec{v}\right) + S_h \tag{4}$$

The component transport equation is:

$$\frac{\partial}{\partial t}(\rho Y_i) + \nabla \cdot (\rho \vec{v} Y_i) = -\nabla \cdot \vec{J}_i + R_i + S_i \tag{5}$$

As the explosion process will generate density and pressure gradients, the ideal gas law is introduced for explosive gas:

$$P = \rho R T \tag{6}$$

where t is the time, ρ is the density, p is the pressure, v is the gas flow rate, $\overline{\overline{\tau}}$ is the stress tensor, μ is the molecular viscosity, I is the unit tensor, k_{eff} is the effective thermal conductivity, and T is the temperature. $\vec{J}_i$ is the diffusion flux of species J, h_j is the enthalpy of species J, S_h is the volumetric heat sources, and R_i is the net rate of production of species by chemical reaction. S_i is the rate of creation by addition from the dispersed phase plus any user-defined source.

In this paper, the Reynolds Averaged Numerical Simulation (RANS) is used and the RNG k-ε turbulence model is introduced [21,23,26]. The RNG k-ε model is derived using a statistical technique known as reformulated group theory [23,33]. It is formally similar to

the Standard Model, and its features make it more accurate and reliable for gas explosion than the standard k-ε model. Due to the violent nature of the explosion, a non-equilibrium wall function is used to facilitate better capture of the turbulence near the wall.

2.2. Combustion Model

Premixed gas explosion is a process of chemical reaction and turbulence interaction, so the introduction of the eddy dissipation conceptual model (EDCM) can reduce the computational requirements while ensuring the accuracy of the results. The eddy dissipation conceptual model (EDCM) is the most accurate and detailed combustion model, which assumes that the turbulence consists of a series of eddies with different scales, and the turbulent kinetic energy is transferred from the large-scale eddies to the small-scale eddies. Chemical reactions all occur in small eddies (Kolmogorov scales), with the reaction time controlled by a combination of the survival time of the small eddies and the time required for the chemical reaction itself [34,35].

The length fraction of the small model is:

$$\xi^* = C_\xi \left(\frac{v\varepsilon}{k^2}\right)^{1/4} \tag{7}$$

The react time in the small scales is:

$$\tau^* = C_\tau \left(\frac{v}{\varepsilon}\right)^{1/2} \tag{8}$$

where $*$ is the small-scale quantities, and C_ξ and C_τ are equal to 2.1377 and 0.4082. v is the kinematic viscosity, k is the turbulence kinetic energy, and ε is the rate of dissipation.

The model can take into account the detailed chemical reaction mechanism in the turbulent reaction, which makes the numerical simulation results more accurate. The detailed chemical reaction mechanism uses a 19-step hydrogen/air combustion reaction mechanism with 9 species [36] as shown in Table 1.

Table 1. Reaction mechanism [36].

No.	Process	A	n	E
1	$H + O_2 \Rightarrow O + OH$	3.55×10^{15}	−0.41	16.60
2	$O + H_2 \Rightarrow H + OH$	5.08×10^{4}	2.67	6.29
3	$H_2 + OH \Rightarrow H_2O + H$	2.16×10^{8}	1.51	3.43
4	$O + H_2O \Rightarrow OH + OH$	2.97×10^{6}	2.02	13.40
5	$H_2 + N_2 \Rightarrow H + H + N_2$	4.58×10^{19}	−1.40	104.38
6	$O + O + N_2 \Rightarrow O_2 + N_2$	6.16×10^{15}	-0.50	0.00
7	$O + H + N_2 \Rightarrow OH + N_2$	4.71×10^{18}	−1.00	0.00
8	$H + OH + N_2 \Rightarrow H_2O + N_2$	3.80×10^{22}	−2.00	0.00
9	$H + O_2 + N_2 \leftrightarrow HO_2 + N_2$	6.37×10^{20}	−1.72	0.52
10	$HO_2 + H \Rightarrow H_2 + O_2$	1.66×10^{13}	0.00	0.82
11	$HO_2 + H \Rightarrow OH + OH$	7.08×10^{13}	0.00	0.30
12	$HO_2 + O \Rightarrow OH + O_2$	3.25×10^{13}	0.00	0.00
13	$HO_2 + OH \Rightarrow H_2O + O_2$	2.89×10^{13}	0.00	−0.50
14	$HO_2 + HO_2 \Rightarrow H_2O_2 + O_2$	4.20×10^{14}	0.00	11.98
15	$H_2O_2 + N_2 \leftrightarrow OH + OH + N_2$	1.20×10^{17}	0.00	45.50
16	$H_2O_2 + H \Rightarrow H_2O + OH$	2.41×10^{13}	0.00	3.97
17	$H_2O_2 + H \Rightarrow H_2 + HO_2$	4.82×10^{13}	0.00	7.95
18	$H_2O_2 + O \Rightarrow OH + HO_2$	9.55×10^{6}	2.00	3.97
19	$H_2O_2 + OH \Rightarrow H_2O + HO_2$	1.00×10^{12}	0.00	0.00

2.3. Geometry and Mesh

The rationality and accuracy of the CFD model are demonstrated using the experimental results. The resource cost of using a 3D model to solve the detailed chemical reaction

mechanism is severe, and it has been proved that a 2D model can successfully predict the propagation of premixed flames in ducts [21,26]. Therefore, this paper indicates an axisymmetric 2D model with a size of 530 mm × 82 mm. The ignition position is in the center of the left wall (coordinate, (0 mm, 0 mm)), with an ignition radius of 5 mm. The sum of the blocking rates of the three obstacles is 1; for more details, see Table 2. The thickness of the obstacles is 10 mm, and their space is 100 mm apart as shown in Figure 1.

Table 2. Blocking rate variable under different configurations.

Obstacle Blocking Rate Gradient (OBG)				
Configuration	BR1	BR2	BR3	Variable
Case1	0.375	0.5	0.625	OBG = +0.125
Case2	0.5	0.5	0.5	OBG = 0
Case3	0.625	0.5	0.375	OBG = −0.125

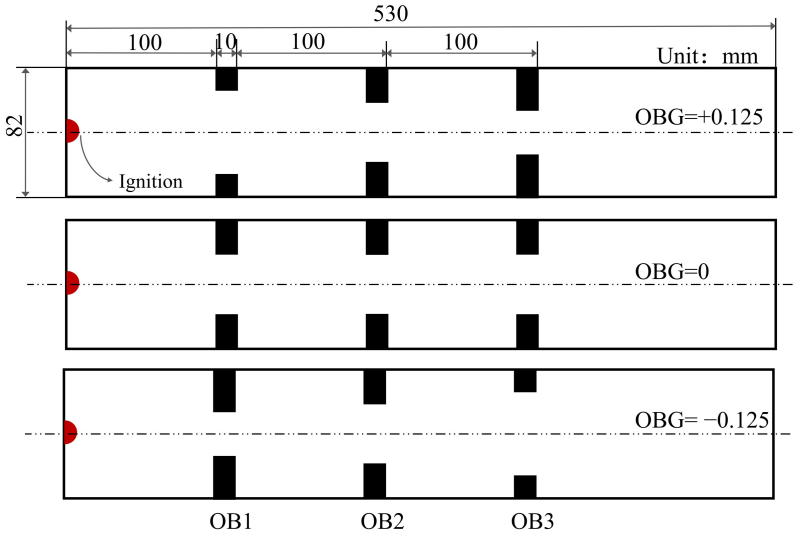

Figure 1. Schematic diagram of obstacles blocking rate gradient (obstacle is abbreviated as OB).

The structured mesh of 0.5 mm is used [37]. To avoid the influence of the mesh size on the simulation results, the flame front is encrypted, applying the adaptive refinement mesh method [38] according to the temperature gradient as shown in Figure 2. The ignition temperature is 2000 K.

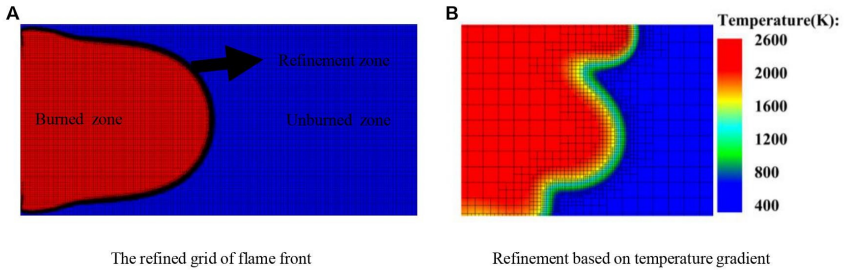

Figure 2. Adaptive mesh refinement. (**A**) Overall. (**B**) Local.

2.4. Initial Condition and Solver

The CFD solver Ansys-Fluent 2021 R1 is operated for numerical solution. The entire computational domain is discretized using the finite volume method for the control equations with a double-precision solver to improve the accuracy of calculations. The premixed hydrogen/air is relatively stationary, and the volume concentration of hydrogen is 30% (the equivalence ratio is 1). The initial temperature is 298 K, and the initial pressure is 1 atm.

The thermal conductivity and dynamic viscosity of mixtures are calculated depending on the ideal gas mixing law. The convection adopts the second-order windward format, and the spatial format is discretized using the central difference format. For complex coupled pressure-velocity calculations, the PISO algorithm is used to couple pressure–velocity, as it can improve the convergence speed compared to the SIMPLE algorithm. Convergence is achieved by ensuring all residuals are dropped at least three magnitudes at every time step [39]. The residuals are less than 1×10^{-6} for the energy equation and less than 1×10^{-5} for other equations. The time step is less than 1/2 of CFL [40] to capture the pressure wave in the duct. The time step determined in this way is already small enough for the study of the interaction between flame front and pressure wave in the duct.

2.5. Validation of Simulation Results

In the simulation of premixed flame explosions, the flame structure and explosion characteristic parameters are often used to evaluate the validation of the numerical model. Therefore, experiments from the literature [41] are selected to verify the accuracy of numerical model. In the simulation, parameters such as pipeline size and ignition position remain consistent with those in the experiment. As shown in Figure 3, the flame structure is compared between numerical simulation and experimental results. It can be observed that the explosion goes through four classical flame shapes during the flame propagation, i.e., spherical stage, finger stage, planar stage, and tulip stage. It is worth noting that as the flame continues to develop, the tulip flame will undergo a significant deformation into a distorted tulip flame [42], after which the tongues of two tulip flames will sink from the center to the wall. The above results are consistent with the experimentally obtained flame characteristics and confirm the reliability of the numerical model.

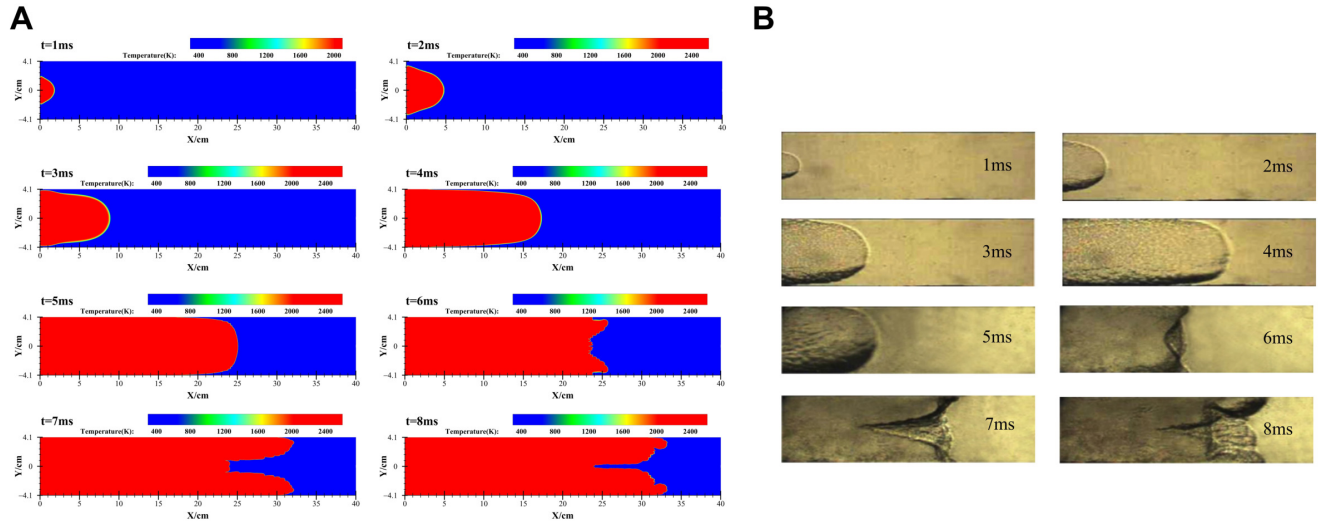

Premixed hydrogen/air explosion flame propagation in closed pipelines from numerical simulation

The flame front of experiment using high-speed cameras

Figure 3. Results of the flame propagation. (**A**) Numerical. (**B**) Experiment [41].

Clanet and Searby [43] firstly proposed the accelerating mechanism of premixed flames in half-open ducts and offered the following empirical formula for calculating the flame characteristic time:

$$t_{\text{sphere}} = (0.10 \pm 0.02)(H/S_{l0}) \quad (9)$$

$$t_{\text{wall}} = (0.26 \pm 0.02)(H/S_{l0}) \quad (10)$$

$$t_{\text{tulip}} = (0.33 \pm 0.02)(H/S_{l0}) \quad (11)$$

where H is the half-height width of the pipe, and S_{lo} is the laminar flame speed, for hydrogen/air with a laminar flame speed of 2.1 m/s when the equivalence ratio is 1.

The flame characteristic time of the experimental results, numerical simulation, and theoretical equations are calculated in Table 3. The numerical results are almost the same as the experiment but slightly larger than the theoretical calculations due to the fact that gas cannot be expanded and flowed to the free end in a closed duct, which leads to the pressure and temperature in the unburned area to be elevated. It further results in the flame propagation speed being smaller and finally leads to overestimating the flame characteristic time.

Table 3. The characteristic time of flame propagation in no-obstacle duct.

Flame Stage	Time Type (ms)	Empirical	Experimental [41]	Numerical
Spherical flame	t_{sphere}	1.95 ± 0.39	2.3	2
Finger flame	t_{wall}	5.08 ± 0.39	4.3	4
Tulip flame	t_{tulip}	6.44 ± 0.39	5.6	5.6

Flame front position and explosion overpressure are essential parameters for evaluating the explosion of premixed flames. Figure 4 shows a comparison of experimental and simulated data. A comparison of the flame front position and explosion overpressure with the explosion time are respectively shown in Figure 4A,B. It should be noted that the flame tip at the centerline of the duct before the flame reversal is taken as the flame front, and the tongue of the fire near the upper wall surface after the flame reversal is taken as the flame front. The pressure monitoring point is 130 mm away from the right end, which is the same as the experiment. Figure 4 illustrates that the experimental results and simulation results are in good agreement. Nevertheless, the numerical results are slightly larger than those of the experiment due to the neglect of the wall heat dissipation and heat radiation in the simulation. Nevertheless, the overall simulation data are better than the results in the existing literature [15,21], especially the flame front results: the average relative error between the experiment and simulation is about 3%.

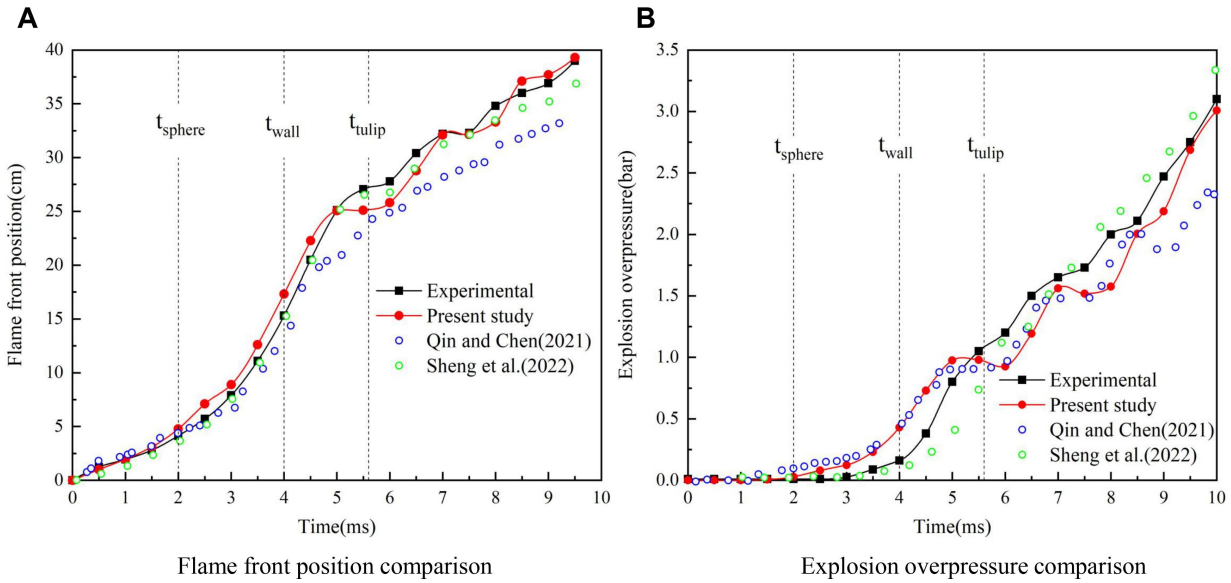

Figure 4. Explosion parameters in the empty duct. (**A**) Flame front position (**B**) Overpressure [15,21].

Based on the above comparisons of the flame position and overpressure, the numerical model used in this study reliably captures the flame propagation and overpressure distribution during the explosion of premixed hydrogen/air in a closed duct, which further demonstrates that the numerical model and calculation method can be adopted to explore the influence of the obstacle gradient arrangement on the flame structure and explosion overpressure.

3. Results and Discussion

3.1. Analysis of Flame Propagation Structure

As shown in Figure 5, after ignition (t < 2.0 ms), the flame front is consistent under different blocking rate gradients, mainly the spherical and finger shapes. At this stage, flame propagation is mainly controlled by the thermal expansion of combustion products, and it is mainly laminar combustion that is not affected by obstacles. When t > 3.0 ms, due to the different arrangement of obstacles inside the pipeline, there is a significant difference in the flame front structure, leading to a transition from combustion to turbulence.

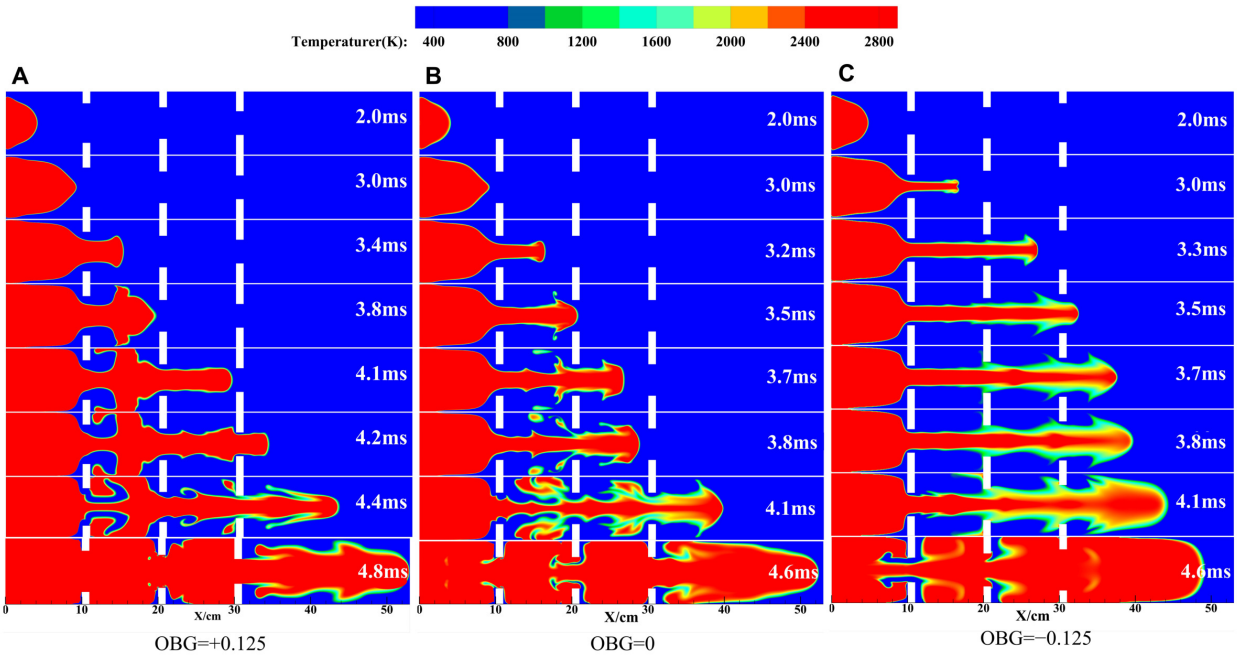

Figure 5. The flame structure over time under different configurations. (**A**) Case-1. (**B**) Case-2. (**C**) Case-3.

When OBG = +0.125, the flame front reaches the first obstacle, causing compression and stretching of the flame front and accelerating to pass. It mainly involves a jet flame (t = 3.0 ms). After passing through obstacles, the flame tip develops longitudinally to form a "small mushroom" structure (t = 3.4 ms). This is due to the Kelvin–Helmholtz instability induced by tangential acceleration at the density interface, resulting in the flame front being backward. When the flame front arrives at the second obstacle, the flame tip undergoes compression and stretching again, owing to the effect of the obstacle, and continues to accelerate through. Both sides of the flame roll back along the wall (t = 3.8 ms). Differently, the deformation of the flame tip is further enhanced due to BR1 < BR2. The flame reaches the third obstacle, and the flames on both sides exhibit a "∃" structure. It should be noted that there is no entrainment at the flame tip at this time, which may be because the flame obtains a greater axial propagation speed (compared to the first obstacle). When t = 4.2 ms, the flame continues to accelerate through the last obstacle, but the upstream flame front wrinkles significantly and surprisingly forms a larger "vortex" flame [44], which is attributed to the interaction between the flame front and the wake vortex of the obstacle (mentioned in Section 3.4). At this point, the flame propagation speed and flame front area reach maximum values. The flame propagates towards the unburned zone (t > 4.2 ms). Overall, more wrinkles are generated on the entire flame front due to the arrangement of obstacles inside the pipeline.

When OBG = 0, the flame structure also undergoes similar changes to Case 1 in the early and late stages. However, BR1 is larger than that at OBG = +0.125, which leads to a larger axial propagation distance of the flame front when passing through the first obstacle

(t = 3.2 ms). As the flame further propagates, the jet flame presents an "umbrella" structure (t = 3.5 ms). It is worth noting that there is no backward suction on either side of the flame, but a pair of symmetrical vortex structures are formed in the flame front. This is mainly attributed to the second obstacle inducing the flame front and generating shear effects and flame instability, resulting in significant folding of the flame front. When the flame completely passes through the second obstacle, the flame front tends to flatten (t = 3.7 ms). This indicates that the interaction between the obstacle wake and flame front becomes stronger, and wake plays an important role in flattening [26].

When OBG = −0.125, an interesting phenomenon is observed during passing through the first obstacle, with a concave front end of the jet flame (t = 3.0 ms). This means that the gas flow speed along the pipeline axis is lower than on both sides. Unlike Case 1 and Case 2, the jet flame always maintains an arc shape. A large and significant temperature gradient is generated on both sides of the flame front. Overall, as the obstacle gradient increases, the flame front always maintains a jet-like shape, and the wrinkles on the flame front become more and more obvious.

3.2. Kinetic Analysis of Flame Propagation Velocity

Under the above working conditions, flame structure variations imply various flame propagation speeds. The curves in Figure 6A,B represent the variations of the flame front position and flame propagation speed over time. Figure 6 reveals three stages of the flame propagation process. The initial phase corresponds to the free explosion stage, during which flame propagation is primarily governed by the thermal expansion of the product, leading to a slow movement of the flame front at laminar flame speed. The flame's inherent instability and the presence of obstacles lead to a transition from laminar to turbulent combustion during the second phase, which is characterized by flame acceleration. In this stage, the flame propagation parameters undergo significant changes, and the position of the flame front gradually becomes more dispersed along each curve as shown in Figure 6A. The larger the gradient of the obstacle, the more pronounced the change in the flame front position. The third phase is the flame deceleration stage, which is influenced by the duct wall and the pressure wave reflection (as in Section 3.3). During this stage, the flame gradually decelerates, and the rate of change of the flame front position slows down over time.

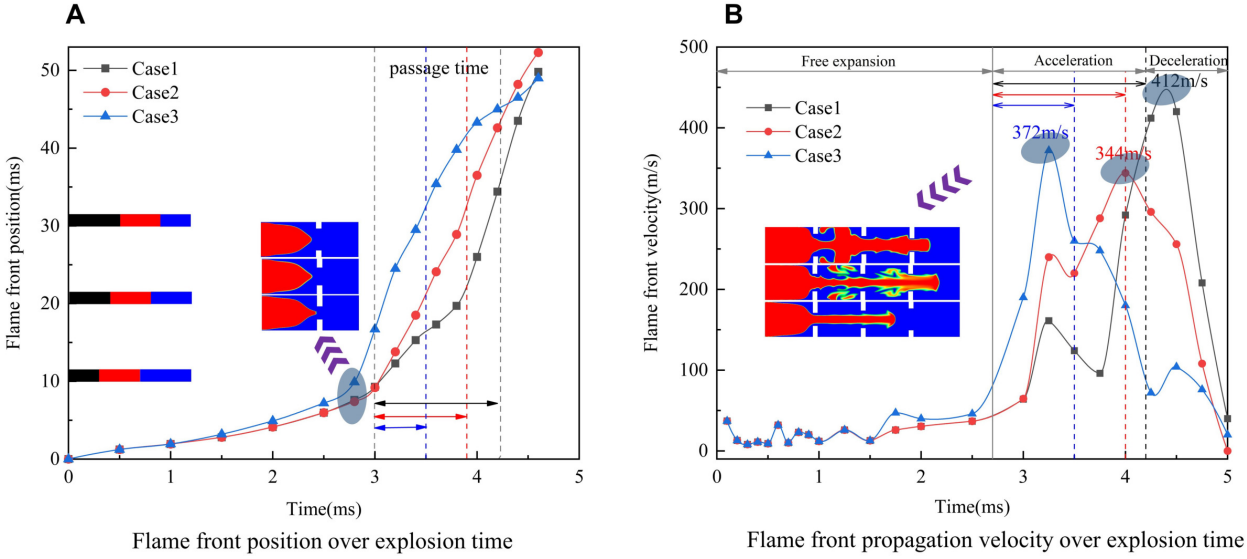

Figure 6. Explosion parameters over time. (**A**) Flame front position (**B**) Propagation velocity.

The overall trend of flame propagation velocity for each working condition consistently follows an initial increase followed by a decrease in Figure 6B. Specifically, when OBG = 0, the maximum flame propagation velocity reaches 344 m/s. However, when OBG = ±0.125,

the values are respectively 372 m/s and 412 m/s, representing 8.1% and 19.8% increases in the maximum flame propagation velocity. It is evident that the obstacle gradient influences the flame propagation velocity differently.

3.3. The Effect on Dynamic Overpressure

When hydrogen is ignited, the high temperature generated by combustion causes the unburned gas in front of the flame to expand. Constrained by the pipeline wall, a certain pressure is generated in the unburned gas ahead, continuously compressing the unburned gas and forming a compression wave. As the flame continues to propagate, the intensity of the compression wave increases, causing the unburned gas to be continuously compressed. At the same time, due to the presence of obstacles in the pipeline, compression waves reflect and repeatedly propagate in the pipeline. With the different obstacle gradients, the overpressure undergoes varied changes as shown in Figure 7.

Overall, as the flame progresses, the overpressure in the pipe gradually increases, and there are obvious high-pressure and low-pressure areas distributed (especially behind obstacles). The distribution of pressure is closely related to the changes in the flame structure, and the direction of the pressure gradient can also have different effects on the flame propagation speed.

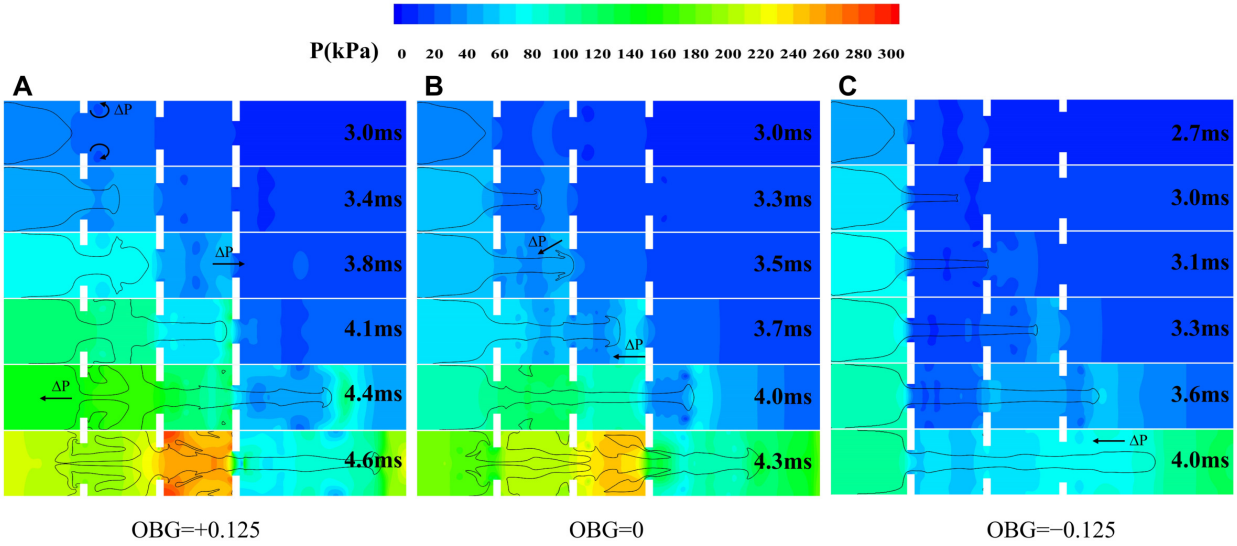

Figure 7. The distribution of overpressure in the obstacle duct. (**A**) Case-1. (**B**) Case-2. (**C**) Case-3.

At OBG = +0.125, when the flame crosses the first obstacle, a low-pressure area is formed behind the obstacle. At this time, the flame is rolled up into a vortex under the driving force of the pressure gradient (as mentioned in Section 3.1). Moreover, clear high- and low-pressure boundaries can be observed at each obstacle, which also means that the flame continues to accelerate towards the unburned zone. As combustion progresses, the overpressure inside the pipeline increases. When the flame reaches the third obstacle, a high pressure zone can be observed near the obstacle, which also means that the flame front is distorted by the influence of the obstacle and reflected waves. When the flame completely passes through all obstacles, it is worth noting that a significant pressure gradient is formed in the ignited zone upstream of the pipeline, causing gas to reflux inside the pipeline. In addition, a pressure gradient direction opposite to the propagation direction is generated at the flame front, indicating that the flame begins to slow down due to the influence of wall reflection waves.

At OBG = 0 and OBG = −0.125, it is also consistent. We can observe that there is a correlation between the structural changes of the flame front, flame propagation speed, and pressure distribution. Especially at OBG = −0.125, when the flame passes through obstacles, the pressure gradient inside the pipe follows the direction of flame propagation,

which also reflects the reason for the continuous acceleration of the flame (mentioned in Section 3.2). Meanwhile, the baroclinic torque will be generated when the pressure and density gradient is formed, resulting in R-T instability. With the action of the R-T instability, the flame front will undergo obvious periodic fold deformation. Overall, the overpressure inside pipe increases with the increase in the obstacle gradient.

The dynamic pressure and growth rate at the monitoring point downstream of the duct with explosion time are plotted under different working conditions as shown in Figure 8. Figure 8A shows the variation curve of the overpressure with explosion time at the downstream monitoring point of the pipeline. When t < 3.0 ms, combustion is not affected by obstacles, and the pressure wave has not yet reached downstream. Then, as the flame passes through the obstacle, the overpressure caused by the obstacle continues to increase. As the flame propagates, the explosion overpressure undergoes a slight oscillation due to collision with compression waves [23]. The increase in flame instability causes the overpressure oscillation.

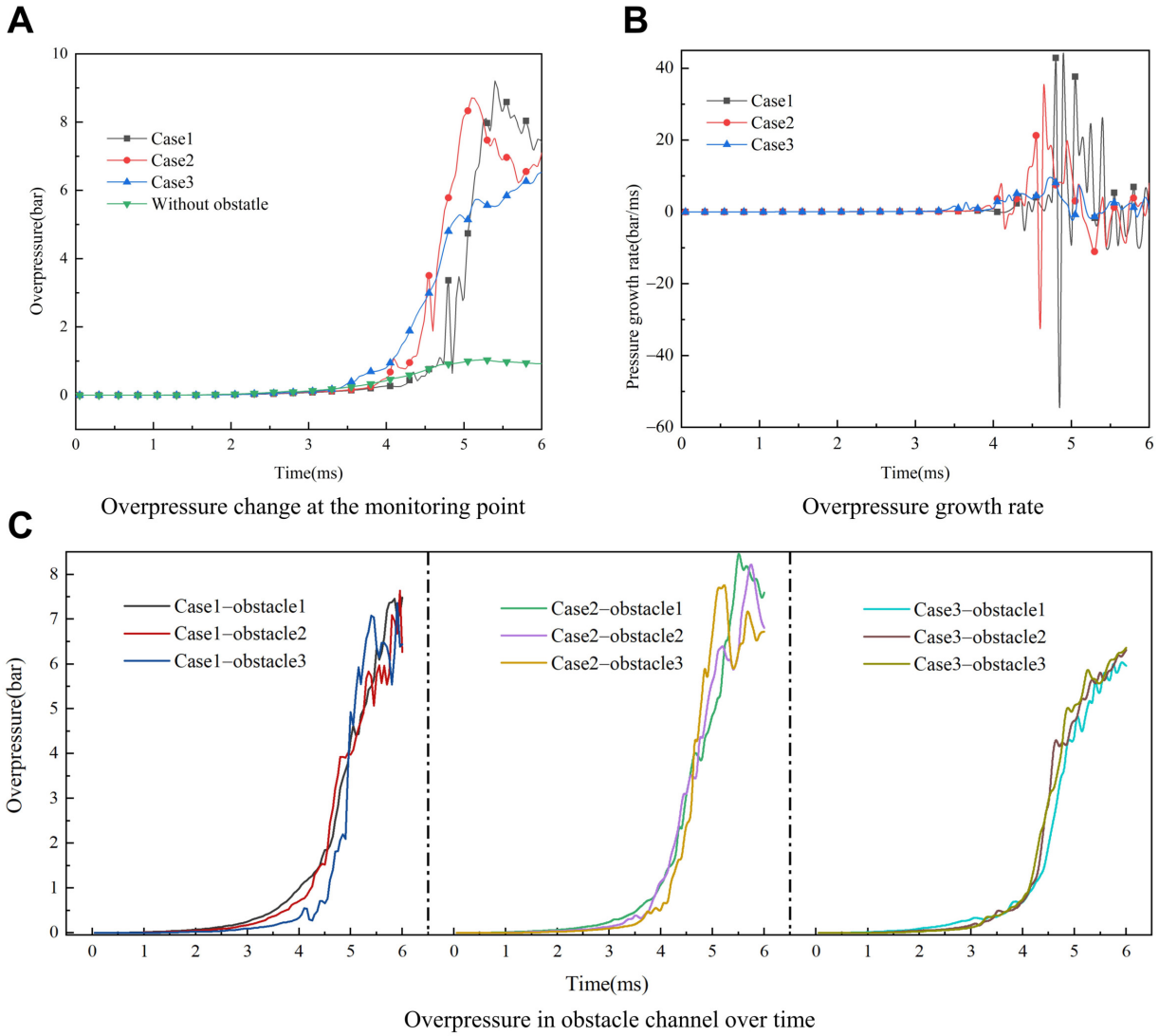

Figure 8. Simulation results of overpressure in obstacle duct. (**A**) Monitoring point. (**B**) Growth rate. (**C**) Obstacle channel.

Figure 8B illustrates a consistent oscillation trend of explosion overpressure in all conditions. It is noteworthy that when OBG = +0.125, the overpressure oscillation amplitude is the largest, with the maximum growth rate reaching 60 bar/s, while the peak overpressure

growth rates are only 40 bar/s and 5 bar/s at OBG = 0 and −0.125, respectively. The greater peak of dynamic overpressure oscillation trend of explosion overpressure means more explosion intensity, consequently triggering heightened explosive damage. To further analyze the effect of different obstacle channels on the explosion overpressure of premixed hydrogen/air, the variation of the explosion pressure of each obstacle channel is plotted in Figure 8C. Similarly, at 3 ms < t < 4 ms, the pressure in the obstacle channel is slowly growing; at 4 ms < t <5 ms, the pressure is suddenly and sharply increased; and at t > 5 ms, the pressure shows a cyclic change of growth followed by a decrease and then an increase. Moreover, the arrangement of the blocking rate gradient to some extent reduces the overpressure value inside the obstacle channels.

3.4. Flow Field under Different Obstacle Gradient Conditions

The changes in the flow field inside the pipe are closely related to the flame propagation process, especially the gas guided flow and velocity. Figure 9 shows the velocity vector and vortex structure of the propagation process.

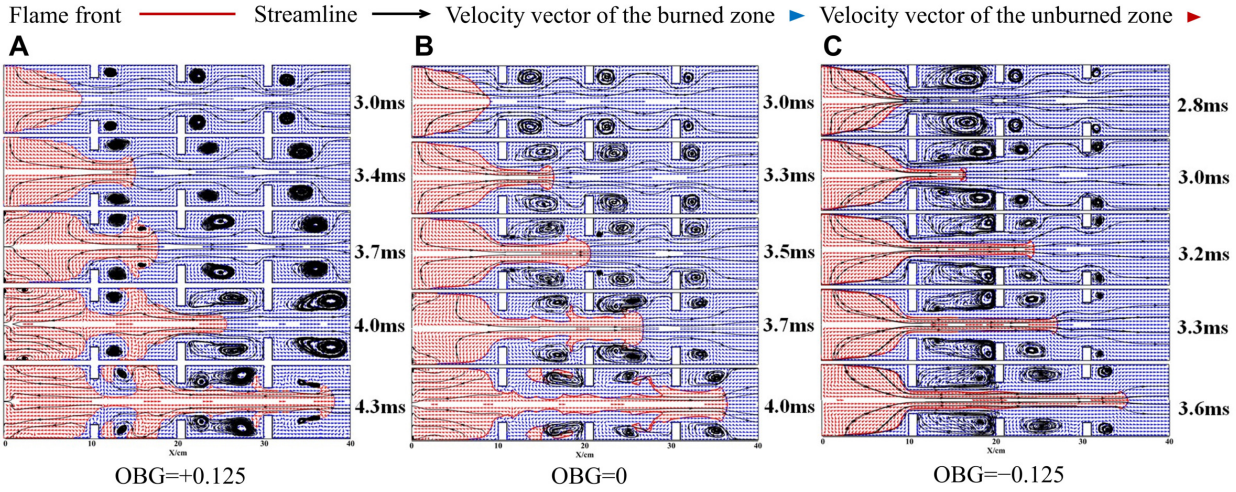

Figure 9. Streamline and velocity vector distribution map in duct. (**A**) Case-1. (**B**) Case-2. (**C**) Case-3.

When the flame front reaches the vicinity of an obstacle, according to the continuity equation, the airflow at the obstacle will be accelerated. Simultaneously affected by turning and shear flow, vortexes are generated on both sides behind the obstacle. Afterwards, under the guidance of flow, the flame accelerates through the channel effected by obstacles and the pipe wall. At this point, the flame front undergoes deformation due to the influence of the vortex, and the flame expands along the outer flow field of the vortex to form a vortex flame. Subsequently, the surface area of the flame front reaches its maximum value. When the flame continues to propagate and continuously passes through obstacles, wrinkles occur on the surface of the flame due to the influence of the airflow, pipe walls, and obstacle channels.

Moreover, the wake vortex of the obstacle further stretches and deforms with the acceleration of the flame, even generating new vortexes. At the same time, it can be observed that the scale of the vortex is positively correlated with the blocking rate of obstacles, and the larger the blocking rate, the larger the scale of the formed vortex. It is worth noting that in OBG = +0.125, when the flame passes through all obstacles, as the flame continues to propagate, the vortex behind the obstacles near the flame front gradually disappears, and a small vortex forms on the surface of the flame front. This change means that the edge of the flame skirt will gradually approach the wall and decelerate to form a flat flame [44]. When flames pass through obstacles, different airflow structures can cause various unstable effects on flame propagation. During the flame acceleration process, low-density products fly towards high-density unburned gases, leading to R-T instability. On

the other hand, the shear effect of vortex and turning flow lead to K-H instability. Overall, vortexes have a significant impact on flame structure deformation and flow field changes.

The vortex can be further quantitatively analyzed by calculating the vorticity ($\vec{\Omega} = \nabla \times \vec{U}$) of the flow field. In Figure 10, the vorticity is symmetrically distributed along the axis and is positive (northern hemisphere) when it flows counterclockwise. In general, the vorticity of the flame tip is approximately zero for different obstacle arrangements. The maximum vorticity is located at obstacle, which is accounted for by the fact that the pressure and velocity vary most dramatically at the obstacle. During the flame propagation process, especially after passing through obstacles, different airflow organization distributions lead to changes in the vortex. In pipelines with different obstacle gradient arrangements, the larger the vorticity, the greater the combustion intensity and turbulence intensity.

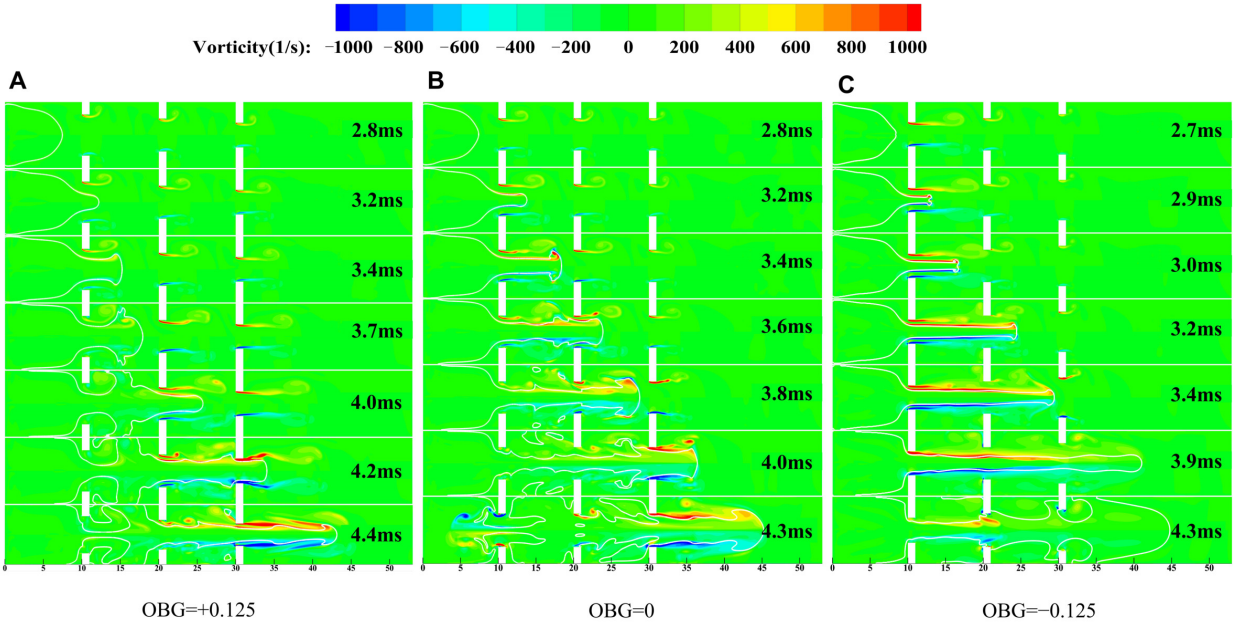

Figure 10. Flow field structure of deflagration flame propagation under different configurations. (**A**) Case-1. (**B**) Case-2. (**C**) Case-3.

The above flow field structure and vortex analyses indicate that the flow field may influence the flame front. In Figure 11, the flow velocity distribution in the flame front's cross-section at different moments under different working conditions is shown. Before the formation of the jet flame, the airflow velocity at the flame front in the tube changes little in the radial direction, and the velocity gradient is slight. At this time, the flame acceleration is mainly caused by thermal expansion and self-instability. However, when the flame passes through the gap between the obstacle and the inner wall of the tube, the radial distribution of the airflow velocity at the flame front changes significantly, which is reflected in the lower radial velocity on the side of the obstacles. Therefore, there is a large radial velocity gradient in the flame front, which is mainly caused by the tail vortex of obstacles. It can be seen from Figure 11 that with the increase in the obstacle gradient, the radial velocity gradient of the flame front airflow is larger, which is related to the positive feedback relationship between the flame propagation velocity, surface area, and tension strength.

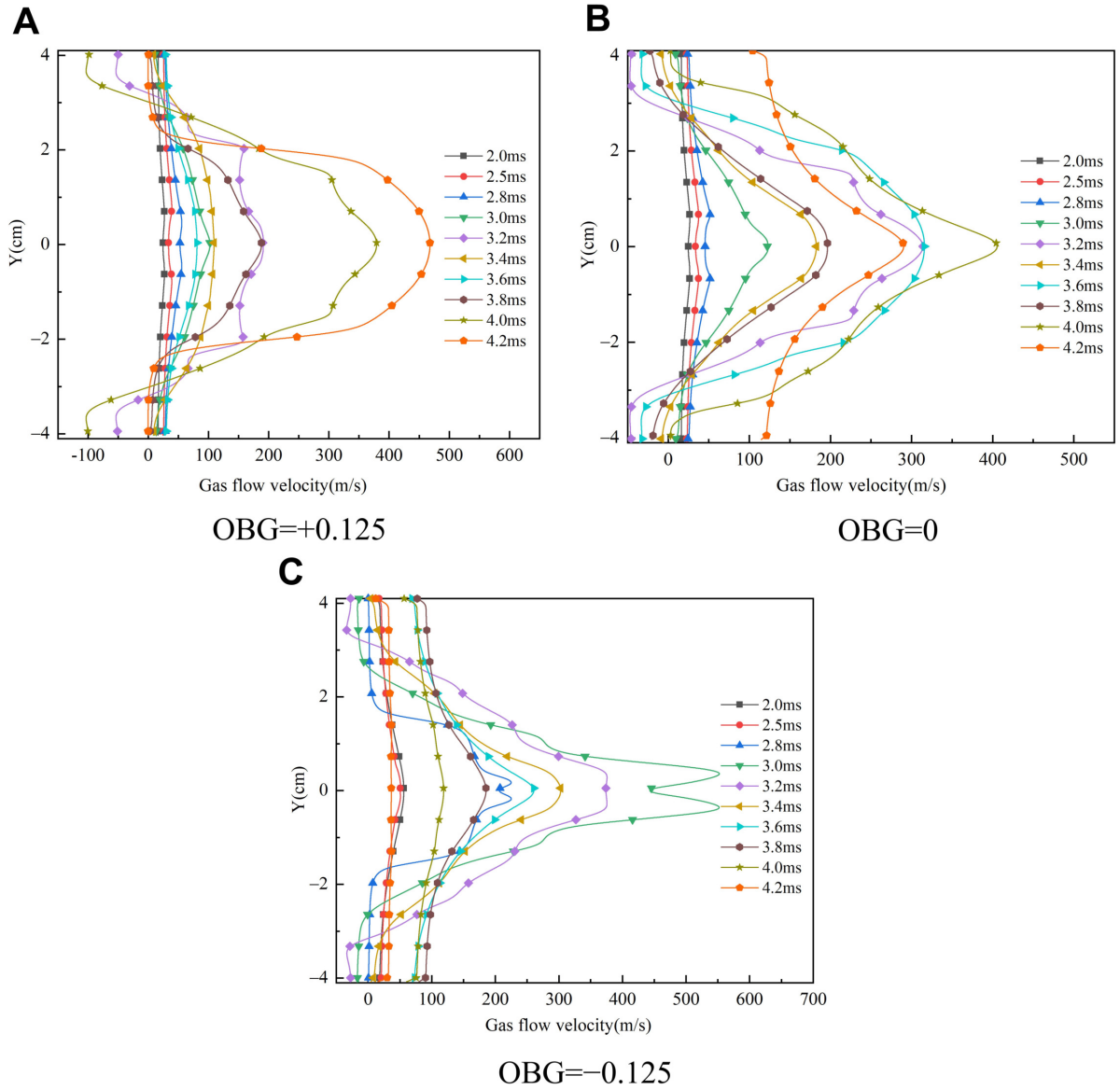

Figure 11. Radial velocity distribution curve of the flame front at different time. (**A**) Case-1 (**B**) Case-2 (**C**) Case-3.

To further investigate the distribution and influence of different blocking rate obstacle channels on the flow velocity, the change in flow velocity at each obstacle channel is shown in Figure 12. All flow velocities at the obstacles experienced similar changes with time. During the laminar phase, the flow velocity is increased slowly. When reaching the obstacle, the flame accelerates into a turbulent phase. When propagating to the downstream region, the reflected wave gradually reduces the flow velocity. In the middle and late stages of flame propagation, the flow velocity reverses due to diffusion of the gas flow to both sides and the reflux effect. Then, the flow velocity oscillates and changes due to the enhancement of the flame instability, etc.

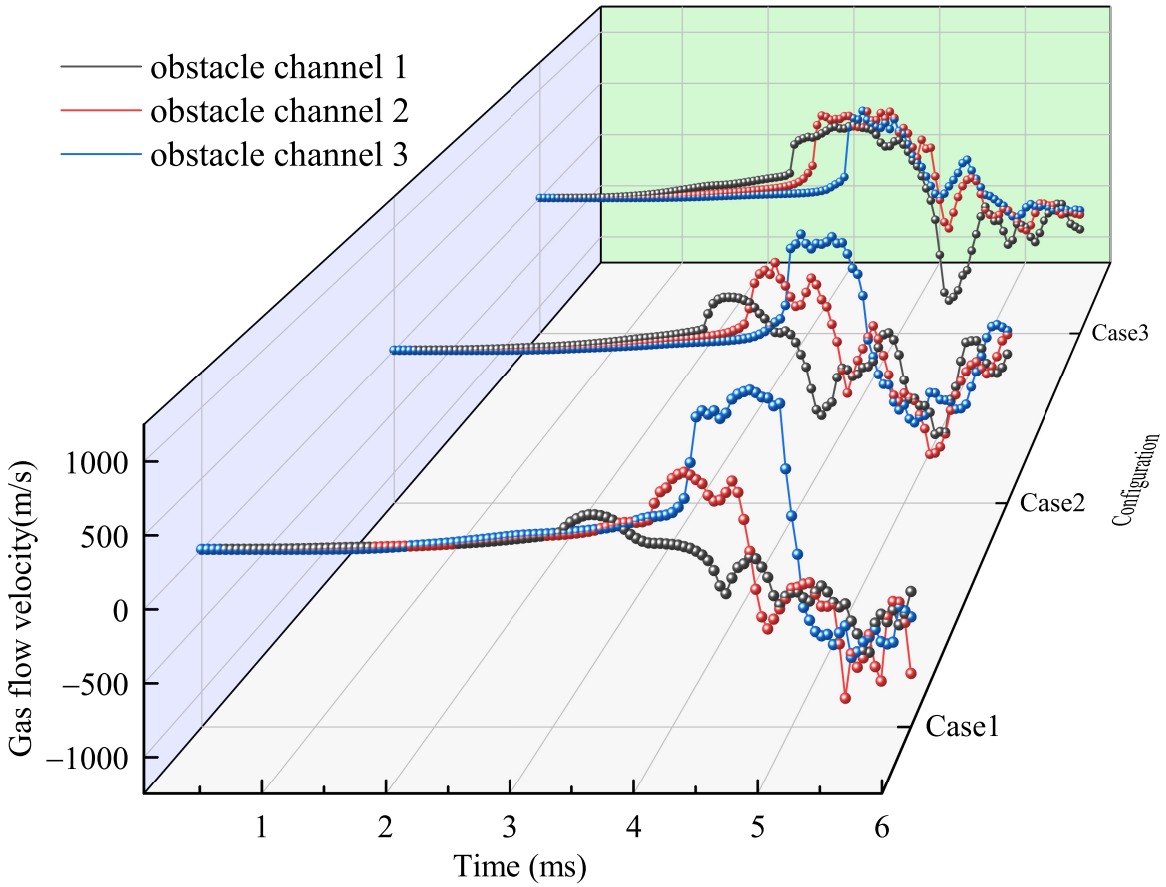

Figure 12. Flow velocity distribution curve over time in each obstacle channel.

The effect of the obstacle gradient on the gas flow acceleration is different. When OBG = +0.125, as the explosion proceeds, the peak of flow velocity in each obstacle channel is 243 m/s, 542 m/s, and 1122 m/s, where the velocity increase is 123%, 107%. As shown in Table 4, it can be found that with the rise in the obstacle gradient, the flow velocity increase amplitude is larger, and even deceleration occurs when OBG = −0.125.

Table 4. Flow velocity in obstacle channel under different configurations.

Configuration	Obstcle1 (m/s)	Obstcle2 (m/s)	Obstcle3 (m/s)	Increase in Flow Velocity
Case1	243	542	1122	123% and 107%
Case2	433	712	922	64% and 29%
Case3	670	759	733	12% and −3%

4. Conclusions

This paper investigates the effects of different obstacle gradients on the flame propagation characteristics of premixed hydrogen/air in a closed chamber. This research result can provide basic simulation data for hydrogen explosion in obstacle pipelines. The following are the main conclusions:

1. The arrangement of the obstacle gradient can change the morphology of the explosion flame in the process. Overall, as the obstacle gradient increases, the flame front always maintains a jet-like shape, and the wrinkles on the flame front become more and more obvious.
2. The blocking rate gradient has different effects on the flame propagation speed, which is enhanced by 8.1% (OBG = −0.125) and 19.8% (OBG = +0.125), respectively. The distribution of pressure is closely related to the changes in the flame structure, and

the direction of the pressure gradient can also have different effects on the flame propagation speed. The blocking rate gradient will decrease the overpressure in obstacle channels to different degrees.

3. An obvious vortex whose size is proportional to the blocking rate of the obstacle will be formed behind the obstacle during the flame propagation process. The vortex plays a key role during flame structure evolution, and more vortexes will be produced on the flame front with the increase in the obstacle gradient when passing channels.
4. The arrangement of obstacles increases the gas flow velocity, and the larger the obstacle gradient, the greater the increase in flow velocity. But deceleration occurs at OBG = −0.125.

For future simulation studies, consideration should be given to the heat exchange between the pipeline wall and the environment to further optimize the numerical model and improve the accuracy of the results. Additionally, the arrangement of obstacle blocking rates needs further enrichment and refinement to explore the effects of various arrangements on the propagation of hydrogen/air premixed flames. More importantly, this simulation was conducted based on small-sized pipes, and future studies should focus on the propagation of premixed flames in obstacle gradient pipelines under more realistic conditions for actual hydrogen transportation and storage.

Author Contributions: Validation, Y.W.; Formal analysis, Y.W.; Investigation, Y.W.; Resources, Y.W.; Writing—original draft, Y.W.; Visualization, Y.W.; Writing—review & editing, S.Z.; Project administration, S.Z.; Supervision, S.Z.; Funding acquisition, S.Z. All authors have read and agreed to the published version of the manuscript.

Funding: This APC was funded by 14th Five Year National Key Plan : NO. 2023YFC3010600.

Data Availability Statement: The data presented in this study are available on request from the corresponding author

Acknowledgments: Thanks the technical support of Chol Hak Han of University of Science

Conflicts of Interest: The authors declare no conflicts of interest.

References

1. Okere, C.J.; Sheng, J.J. Review on Clean Hydrogen Generation from Petroleum Reservoirs: Fundamentals, Mechanisms, and Field Applications. *Int. J. Hydrogen Energy* **2023**, *48*, 38188–38222. [CrossRef]
2. Salehi, F.; Abbassi, R.; Asadnia, M.; Chan, B.; Chen, L. Overview of Safety Practices in Sustainable Hydrogen Economy—An Australian Perspective. *Int. J. Hydrogen Energy* **2022**, *47*, 34689–34703. [CrossRef]
3. Norazahar, N.; Ambikabathy, T.M.; Kasmani, R.M.; Ahmad, A.; Jalil, A.A.; Abdullah, T.A.T.; Kamaroddin, M.F.A. Hydrogen Application and Its Safety: An Overview of Public Perceptions and Acceptance in Malaysia. *Process Saf. Environ. Prot.* **2023**, *180*, 686–698. [CrossRef]
4. Yang, Y.; Wu, Z.; Yao, J.; Guo, T.; Yang, F.; Zhang, Z.; Ren, J.; Jiang, L.; Li, B. An Overview of Application-Oriented Multifunctional Large-Scale Stationary Battery and Hydrogen Hybrid Energy Storage System. *Energy Rev.* **2024**, *3*, 100068. [CrossRef]
5. Li, J.C.; Xu, H.; Zhou, K.; Li, J.Q. A Review on the Research Progress and Application of Compressed Hydrogen in the Marine Hydrogen Fuel Cell Power System. *Heliyon* **2024**, *10*, e25304. [CrossRef]
6. Goswami, R.; Sun, B. Study on Vapour Dispersion and Explosion from Compressed Hydrogen Spill: Risk Assessment on a Hydrogen Plant. *Int. J. Hydrogen Energy* **2022**, *47*, 41195–41207. [CrossRef]
7. Zhang, T.; Jiang, Y.; Wang, S.; Pan, X.; Hua, M.; Wang, Z.; Wang, Q.; Li, Y.; Jiang, J. Numerical Study on the Flow Characteristics of Pressurized Hydrogen Leaking into the Confined Space through Different Shaped Orifices. *Int. J. Hydrogen Energy* **2022**, *47*, 35527–35539. [CrossRef]
8. Guo, L.; Su, J.; Wang, Z.; Shi, J.; Guan, X.; Cao, W.; Ou, Z. Hydrogen Safety: An Obstacle That Must Be Overcome on the Road towards Future Hydrogen Economy. *Int. J. Hydrogen Energy* **2024**, *51*, 1055–1078. [CrossRef]
9. Bivol, G.; Golovastov, S.; Golub, V. Effect of Channel Geometry and Porous Coverage on Flame Acceleration in Hydrogen–Air Mixture. *Process Saf. Environ. Prot.* **2021**, *151*, 128–140. [CrossRef]
10. Wang, W.; Cheng, Y.; Wang, R.; Wang, H.; Wang, Q.; Liu, R.; Ma, H. Flame Behaviors and Overpressure Characteristics of the Unconfined Acetylene-Air Deflagration. *Energy* **2022**, *246*, 123380. [CrossRef]
11. Cao, W.; Li, W.; Zhang, L.; Chen, J.; Yu, S.; Zhou, Z.; Zhang, Y.; Shen, X.; Tan, Y. Flame Characteristics of Premixed H2-air Mixtures Explosion Venting in a Spherical Container through a Duct. *Int. J. Hydrogen Energy* **2021**, *46*, 26693–26707. [CrossRef]

12. Cao, W.; Zhou, Z.; Li, W.; Zhao, Y.; Yang, Z.; Zhang, Y.; Ouyang, S.M.; Shu, C.M.; Tan, Y. Under-Expansion Jet Flame Propagation Characteristics of Premixed H2/Air in Explosion Venting. *Int. J. Hydrogen Energy* **2021**, *46*, 38913–38922. [CrossRef]
13. Shirvill, L.; Roberts, T.; Royle, M.; Willoughby, D.; Sathiah, P. Experimental Study of Hydrogen Explosion in Repeated Pipe Congestion—Part 2: Effects of Increase in Hydrogen Concentration in Hydrogen-Methane-Air Mixture. *Int. J. Hydrogen Energy* **2019**, *44*, 3264–3276. [CrossRef]
14. Shen, R.; Jiao, Z.; Parker, T.; Sun, Y.; Wang, Q. Recent Application of Computational Fluid Dynamics (CFD) in Process Safety and Loss Prevention: A Review. *J. Loss Prev. Process Ind.* **2020**, *67*, 104252. [CrossRef]
15. Sheng, Z.; Yang, G.; Li, S.; Shen, Q.; Sun, H.; Jiang, Z.; Liao, J.; Wang, H. Modeling of Turbulent Deflagration Behaviors of Premixed Hydrogen-Air in Closed Space with Obstacles. *Process Saf. Environ. Prot.* **2022**, *161*, 506–519. [CrossRef]
16. Sun, X.; Lu, S. Effect of Obstacle Thickness on the Propagation Mechanisms of a Detonation Wave. *Energy* **2020**, *198*, 117186. [CrossRef]
17. Boeck, L.; Lapointe, S.; Melguizo-Gavilanes, J.; Ciccarelli, G. Flame Propagation across an Obstacle: OH-PLIF and 2-D Simulations with Detailed Chemistry. *Proc. Combust. Inst.* **2017**, *36*, 2799–2806. [CrossRef]
18. Yang, X.; Yu, M.; Zheng, K.; Luan, P.; Han, S. An Experimental Study on Premixed Syngas/Air Flame Propagating across an Obstacle in Closed Duct. *Fuel* **2020**, *267*, 117200. [CrossRef]
19. Xiao, H.; Oran, E.S. Flame Acceleration and Deflagration-to-Detonation Transition in Hydrogen-Air Mixture in a Channel with an Array of Obstacles of Different Shapes. *Combust. Flame* **2020**, *220*, 378–393. [CrossRef]
20. Oh, K.H.; Kim, H.; Kim, J.B.; Lee, S.E. A Study on the Obstacle-Induced Variation of the Gas Explosion Characteristics. *J. Loss Prev. Process Ind.* **2001**, *14*, 597–602. [CrossRef]
21. Qin, Y.; Chen, X. Flame Propagation of Premixed Hydrogen-Air Explosion in a Closed Duct with Obstacles. *Int. J. Hydrogen Energy* **2021**, *46*, 2684–2701. [CrossRef]
22. Elshimy, M.; Ibrahim, S.; Malalasekera, W. Numerical Studies of Premixed Hydrogen/Air Flames in a Small-Scale Combustion Chamber with Varied Area Blockage Ratio. *Int. J. Hydrogen Energy* **2020**, *45*, 14979–14990. [CrossRef]
23. Qin, Y.; Chen, X. Study on the dynamic process of in-duct hydrogen-air explosion flame propagation under different blocking rates. *Int. J. Hydrogen Energy* **2022**, *47*, 18857–18876. [CrossRef]
24. Mei, Y.; Shuai, J.; Li, Y.; Zhou, N.; Ren, W.; Ren, F. Flame Acceleration Process of Premixed Hydrogen in Confined Space with Different Obstacle Shapes. *Fuel* **2023**, *334*, 126624. [CrossRef]
25. Jiang, Y.; Gao, W.; Sun, Z.; Liang, B.; Zhang, K.; Li, Y. Experimental and Numerical Study on Explosion Behavior of Hydrogen-Air Mixture in an Obstructed Closed Chamber. *Int. J. Hydrogen Energy* **2024**, *49*, 1032–1045. [CrossRef]
26. Wang, S.; Xiao, G.; Duan, Y.; Mi, H. Effect of Obstacle Arrangement on Premixed Hydrogen Flame: Eddy-dissipation Concept Model Based Numerical Simulation. *Int. J. Hydrogen Energy* **2023**, *48*, 16445–16456. [CrossRef]
27. Xiu, Z.; Liu, Z.; Li, P.; Hao, B.; Li, M.; Zhao, Y.; Cai, P. Effects of Combined Obstacles on Deflagration Characteristics of Hydrogen-Air Premixed Gas. *Int. J. Hydrogen Energy* **2023**, *79*, 31008–31021. [CrossRef]
28. Zheng, K.; Jia, Q.; Ma, Z.; Xing, Z.; Hao, Y.; Yu, M. Experimental and Numerical Investigation on the Premixed Methane/Air Flame Propagation in Duct with Obstacle Gradients. *Process Saf. Environ. Prot.* **2023**, *178*, 893–904. [CrossRef]
29. Wang, S.; Xiao, G.; Feng, Y.; Mi, H. Investigation of Premixed Hydrogen/Methane Flame Propagation and Kinetic Characteristics for Continuous Obstacles with Gradient Barrier Ratio. *Energy* **2023**, *267*, 126620. [CrossRef]
30. Krishnamoorthy, G.; Mulenga, L. Impact of Radiative Losses on Flame Acceleration and Deflagration to Detonation Transition of Lean Hydrogen-Air Mixtures in a Macro-Channel with Obstacles. *Fluids* **2018**, *3*, 104. [CrossRef]
31. Liu, D.; Liu, Z.; Xiao, H. Flame Acceleration and Deflagration-to-Detonation Transition in Narrow Channels Filled with Stoichiometric Hydrogen-Air Mixture. *Int. J. Hydrogen Energy* **2022**, *47*, 11052–11067. [CrossRef]
32. Shen, T.; Li, M.; Xiao, H. Propagation of Premixed Hydrogen-Air Flame Initiated by a Planar Ignition in a Closed Tube. *Int. J. Hydrogen Energy* **2022**, *47*, 4903–4915. [CrossRef]
33. Yakhot, V.; Orszag, S.A. Renormalization Group Analysis of Turbulence. I. Basic Theory. *J. Sci. Comput.* **1986**, *1*, 3–51. [CrossRef]
34. Magnussen, B.F.; Hjertager, B.H. On Mathematical Modeling of Turbulent Combustion with Special Emphasis on Soot Formation and Combustion. *Symp. Int. Combust.* **1977**, *16*, 719–729. [CrossRef]
35. Mansourian, M.; Kamali, R. Modifying the Constant Coefficients of Eddy-dissipation Concept Model in Moderate or Intense Low-Oxygen Dilution Combustion Using Inverse Problem Methodology. *Acta Astronaut.* **2019**, *162*, 546–554. [CrossRef]
36. Li, J.; Zhao, Z.; Kazakov, A.; Dryer, F.L. An Updated Comprehensive Kinetic Model of Hydrogen Combustion. *Int. J. Chem. Kinet.* **2004**, *36*, 566–575. [CrossRef]
37. Zhou, G.; Kong, Y.; Qian, X.; Zhang, Q.; Ma, Y.; Wu, D. Explosion Dynamics and Sensitivity Analysis of Blended LPG/DME Clean Fuel Promoted by H2 in a Confined Elongated Space. *Fuel* **2023**, *331*, 125816. [CrossRef]
38. Khodadadi Azadboni, R.; Heidari, A.; Boeck, L.R.; Wen, J.X. The Effect of Concentration Gradients on Deflagration-to-Detonation Transition in a Rectangular Channel with and without Obstructions—A Numerical Study. *Int. J. Hydrogen Energy* **2019**, *44*, 7032–7040. [CrossRef]
39. Nguyen, T.; Strebinger, C.; Bogin, G.; Brune, J. A 2D CFD Model Investigation of the Impact of Obstacles and Turbulence Model on Methane Flame Propagation. *Process Saf. Environ. Prot.* **2021**, *146*, 95–107. [CrossRef]
40. Xiao, H.; Sun, J.; Chen, P. Experimental and Numerical Study of Premixed Hydrogen/Air Flame Propagating in a Combustion Chamber. *J. Hazard. Mater.* **2014**, *268*, 132–139. [CrossRef]

41. Xiao, H.; An, W.; Duan, Q.; Sun, J. Dynamics of Premixed Hydrogen/Air Flame in a Closed Combustion Vessel. *Int. J. Hydrogen Energy* **2013**, *38*, 12856–12864. [CrossRef]
42. Xiao, H.; Makarov, D.; Sun, J.; Molkov, V. Experimental and Numerical Investigation of Premixed Flame Propagation with Distorted Tulip Shape in a Closed Duct. *Combust. Flame* **2012**, *159*, 1523–1538. [CrossRef]
43. Clanet, C.; Searby, G. On the "tulip flame" phenomenon. *Combust. Flame* **1996**, *105*, 225–238. [CrossRef]
44. Sheng, Z.; Yang, G.; Gao, W.; Li, S.; Shen, Q.; Sun, H. Study on the Dynamic Process of Premixed Hydrogen-Air Deflagration Flame Propagating in a Closed Space with Obstacles. *Fuel* **2023**, *334*, 126542. [CrossRef]